CORA Cork Open Research Archive
Cartlann Taighde Oscailte Chorcaí

Title	Cell formation in stanogermanides using pulsed laser thermal anneal on Ge0.91Sn0.09
Authors	Galluccio, Emmanuele;Mirabelli, Gioele;Harvey, Alan;Conroy, Michele;Napolitani, Enrico;Duffy, Ray
Publication date	2020-08-26
Original Citation	Galluccio, E., Mirabelli; G., Harvey, A., Conroy, M., Napolitani, E. and Duffy, R. (2020) 'Cell formation in stanogermanides using pulsed laser thermal anneal on Ge0.91Sn0.09', Materials Science in Semiconductor Processing, 121, 105399 (5pp). doi: 10.1016/j.mssp.2020.105399
Type of publication	Article (peer-reviewed)
Link to publisher's version	10.1016/j.mssp.2020.105399
Rights	© 2020, Elsevier Ltd. All rights reserved. This manuscript version is made available under the CC BY-NC-ND 4.0 license. - https://creativecommons.org/licenses/by-nc-nd/4.0/
Download date	2026-11-07 08:46:55
Item downloaded from	https://hdl.handle.net/10468/11581

UCC
University College Cork, Ireland
Coláiste na hOllscoile Corcaigh

Cell formation in stanogermanides using pulsed laser thermal anneal on $Ge_{0.91}Sn_{0.09}$

Emmanuele Galluccio,[1] Gioele Mirabelli,[1] Alan Harvey,[2] Michele Conroy,[2]
Enrico Napolitani,[3] Ray Duffy.[1]

[1] Tyndall National Institute, University College Cork, Lee Maltings, Cork, Ireland.
[2] Department of Physics, Bernal Institute, University of Limerick, Ireland.
[3] Dipartimento di Fisica e Astronomia, Università degli Studi di Padova, Via Marzolo 8, 35131 Padova, Italy.

ABSTRACT:

Pulsed laser thermal annealing (LTA) has been thoroughly investigated for the formation of low-resistance stanogermanide contacts on $Ge_{0.91}Sn_{0.09}$ substrates. Three different metals (Ni, Pt, and Ti) were characterized using a wide laser energy density range (100-500 mJ/cm^2). Electrical performance, surface quality, cross-sectional crystallographic, and elemental analysis have been systematically examined in order to identify the ideal process window. Electrical characterization showed that the samples processed by LTA had lower resistance variability compared with the rapid thermal anneal (RTA) counterpart. Among the three metals used, Ni and Pt were the most promising candidates for future sub-nm applications based on the low resistance values. The stanogermanide alloys suffered a high degeneration as the LTA thermal budget increased. Cross-sectional elemental analysis showed a highly unusual Sn segregation effect, particularly for high LTA energy densities, where vertical columns of Sn-rich alloy were formed, also known as cell formation, similar to that seen for Sb hyperdoping of Si when using LTA. This effect is linked to solid solubility and distribution coefficient of Sn in Ge, as well as the velocity of the liquid-solid interface during crystallization as the samples cool.

Keywords- $Ge_{(1-x)}Sn_{(x)}$, laser thermal annealing, liquid-solid reactions, stanogermanides, resistance, solid solubility.

I. INTRODUCTION

The aim to achieve low resistance contact alloys on semiconductor materials such as Si (i.e. silicides) and Ge (i.e. germanides) has been well-studied in the recent past [1-5]. Several papers highlighted electrical performance and structural features as a function of the alloy metal, outlining the most promising material to obtain low resistance contacts. As Ni was found to be the metal with lowest contact resistance for Ge [6], most of previous works on $Ge_{1-x}Sn_x$ were focused on NiGeSn (nickelstanogermanide) [7-9]. Theoretical studies on stanogermanides have also assisted the experimental work [10-12], however the choice of optimum process flow, alloy, and formation thermal treatment are still open questions.

The previous stanogermanide reports present in literature have a common denominator, the contact alloy formation has been achieved using rapid thermal annealing (RTA). In particular to improve the stanogermanide performance enlarging the thermal window budget different experiments have been proposed; Quintero et al.[13] proposed the alloying of Ni with Pt or Co, Wan et al. [14] suggested the addition of a Pt interlayer while the usage of Ti-based stanogermanides instead of Ni was discussed by Wu et al. [15]. Nevertheless, laser thermal annealing (LTA) has recently proven to have enhanced thermal budget control, leading to an ever increasing interest in it for the formation of nanometric devices. LTA is able to localize a laser spot in a precise area without affecting the surrounding regions [16], while also using timescales that limit the thermal diffusion into the substrate, meaning the heat applied is confined to the top layers of the sample under study. Therefore considering the limited thermal budget of $Ge_{(1-x)}Sn_{(x)}$ alloy due to the material metastability and the Sn segregation on to the surface, the LTA technique might represent a valuable resource for the realization of new FET device architectures.

Specifically for Ge, LTA has been used in multiple works showing impressive results [16-19], while for $Ge_{1-x}Sn_x$ LTA has been used only in the study of the epilayer growth [20, 21].

Therefore as the $Ge_{1-x}Sn_x$ contact formation is still an immature field. This work aims to thoroughly investigate stanogermanide contact formation using LTA. The present investigation is on $Ge_{0.91}Sn_{0.09}$ contact formation as a function of three different metals, namely Ni, Pt and Ti.

II. EXPERIMENTAL DETAILS

Fig. 1 shows a schematic illustration of the process flow used in this work. The starting material comprised of a nominally un-doped epi layer of $Ge_{0.91}Sn_{0.09}$ (1.2 µm thick) on un-doped virtual substrate of Ge (700 nm) provided by IQE. On each sample, the $Ge_{0.91}Sn_{0.09}$ surface was first cleaned using a standard Ge recipe to remove the surface contamination, followed by a de-ionized water step to remove the water-soluble GeO_2. There may be some residual sub-oxide layer, since the material is highly sensitive to air exposure. Note that in literature it has been reported that the presence of a low amount of native oxide does not inhibit the germanidation process [22]. Samples were immersed for 30 sec each in acetone and then in isopropyl alcohol (IPA), and finally rinsed with deionized water. 10 nm of either Ni, Ti or Pt, was deposited on samples using a FC2000 electron beam evaporator at a pressure of 5×10^{-7} Torr. To ensure uniform coverage, metals were evaporated with a low rate; Ni and Pt were evaporated at a rate of 0.2 nm/s while the Ti at a rate of 0.1 nm/s. Furthermore, since to date many manuscripts reported the stanogermanide contact analysis without applying any additional capping layer on top of the metal layer the same approach has been used also in this work.

After metal deposition, samples underwent LTA using an excimer KrF laser (Coherent COMPex 201F) equipped with a beam homogeneizer, emitting light at $\lambda = 248$ nm with 22 ns pulse duration, over a square spot 5×5 mm^2 with 2% uniformity. The energy density range was 100-500 mJ/cm^2 in order to have a wide process window.

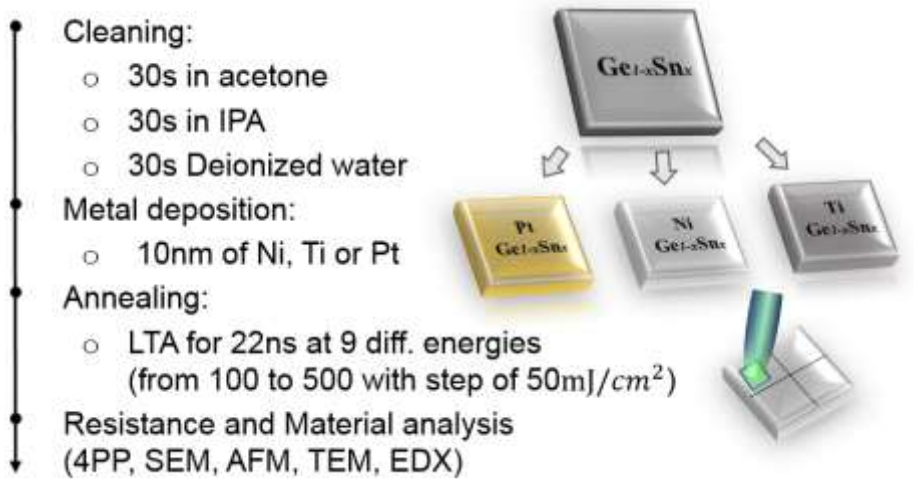


Figure 1: Schematic representation of the stanogermanide process flow in this work.

Concerning material characterization, several techniques have been used to inspect the surface and alloy features. Scanning Electron Microscopy (SEM), Atomic Force Microscopy (AFM), cross sectional Transmission Electron Microscopy (TEM) and Electron Dispersive X-ray (EDX) spectroscopy have been performed on the samples. A SEM investigation was carried out on a Zeiss Supra55VP, while the AFM analysis, considering a 5×5 μm^2 area, was performed in tapping/non-contact mode at room temperature with the Veeco Multi-mode V-AFM.

Cross section samples, needed for TEM analysis, were prepared by FEI's Dual Beam Helios Nanolab Focused ion beam system. Three different layers of protective materials were used, respectively C and Pt deposited by electron beam, and a C layer obtained by ion beam. Bright field mode cross sectional transmission electron microscopy (XTEM) was done in a JEOL2100 HRTEM operated at 200 kV. Scanning transmission electron microscopy (STEM) high-angle annular dark-field (HAADF) imaging and EDX spectroscopy was performed using a Thermo-Fisher Scientific double tilt TEM holder in the Thermo-Fisher Scientific FEI double aberration- corrected monochromated Titan Themis Z. The microscope was operated at 300 kV. Finally a four point probe (4PP) measurement was carried out using a LUCAS LABS-S-302-4. Due to the limited area involved in the LTA process, each sample was analysed in the two diagonals of the square area to extract the average resistance.

III. RESULTS & DISCUSSION

Figure 2 shows the sheet resistance measured as a function of the different metals used (Ni, Pt or Ti). Sheet resistance was probed by Van der Pauw electrical measurements on 5 × 5 m x m^2 samples using a four-point probe system. Due to the small dimensions of the samples (limited by the laser spot size), the accuracy on the measured sheet resistance is 10%. In literature reports, although using RTA as the formation anneal, Ni showed the best performance for Ge [2] and $Ge_{1-x}Sn_x$ [12], while in this work within the LTA power range investigated, PtGeSn shows both the lowest and the highest resistance values.

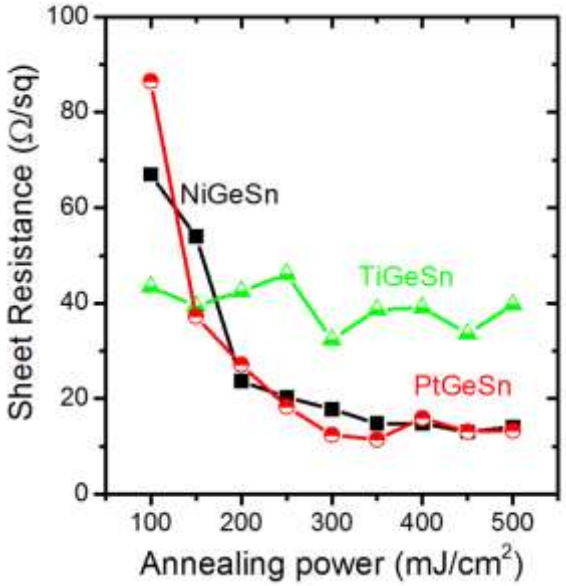


Figure 2: Sheet Resistance for Ni, Ti and Pt stanogermanides as a function of the energy density using laser thermal annealing.

A noteworthy decrease in resistance is observed as the LTA energy density is increased. This might be explained considering the thickness increase of the stanogermanide layer; indeed, the higher energy density of the laser increases the melt depth, causing a thicker stanogermanide to form via a liquid-solid reaction, and so a reduction in the material resistance. Ni and Pt, highlighted respectively with black and red curves, show roughly the same trend, even if Pt has a pronounced deflection up to 350 mJ/cm^2 compared to Ni. Conversely for Ti, displayed in green, higher resistance values have been obtained compared with Ni and Pt

counterparts. The values achieved in the case of Ti might result from possible O incorporation during the alloy formation, as Ti has a strong tendency to oxidise when exposed to the ambient. Compared with previous data obtained using RTA [12] the results achieved by LTA show less variability, and thus tighter process control. We hypothesize that the small fluctuation reached with LTA is strictly related to the ability to melt the underlying $Ge_{0.91}Sn_{0.09}$ with a high degree of precision. Although the comparison between the RTA and LTA methodologies show interesting trends, the exact differences obtained might come from several morphological and processing preparation variances, then further study has to be undertaken to explain the discrepancies.

To characterize the surface quality as a function of the different metals and laser energy density, all the samples have been analysed in the optical microscope and SEM. From the optical microscope analysis a surface transformation was clearly visible, via a colour change, as a function of the LTA energy density, while from SEM images it appeared that PtGeSn and TiGeSn had a greater tendency to have surface texture or to agglomerate at higher laser energy densities.

Subsequently selected samples were examined by XTEM analysis. Figure 3 shows a representative set of images obtained showing NiGeSn as a function of LTA energy density. The stanogermanide layer thickness grew as the LTA energy density increases, as expected. Nevertheless the thickness at a specific LTA energy density was not homogeneous among the NiGeSn, PtGeSn, and TiGeSn samples, which was related to how each metal reflects or absorbs the incident LTA energy. Each metal respectively formed layers with different thickness; NiGeSn (70-420 nm); PtGeSn (50-280 nm) TiGeSn (150-700 nm). If, from one perspective the thickness increase could lead to lower resistance, from the other side, the samples showed a drastic Sn segregation and defect formation within the stanogermanide layers at high LTA

energy density. Ni and Pt stanogermanide layers were inclined to degrade above 250 mJ/cm^2 while Ti stanogermanide showed Sn segregation above 200 mJ/cm^2.

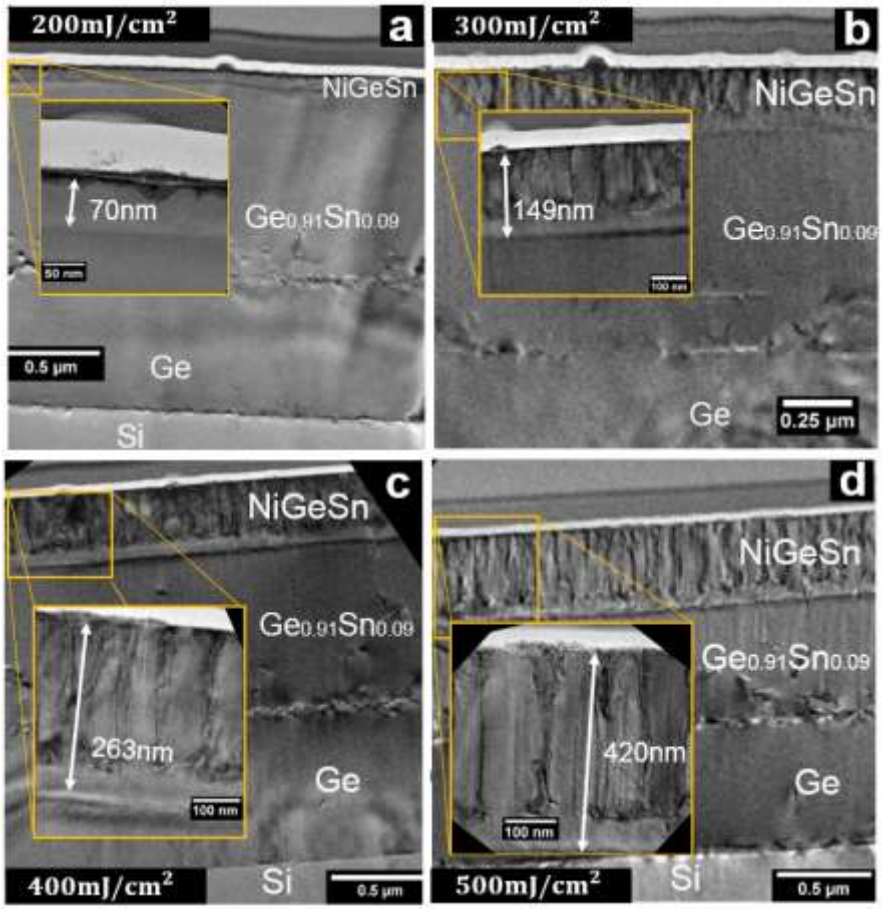


Figure 3: Representative TEM inspection of NiGeSn samples formed by different LTA energy density, to outline the formation of stanogermanide layers as a function of the energy; (a) 200 mJ/cm^2, (b) 300 mJ/cm^2, (c) 400 mJ/cm^2, (d) 500 mJ/cm^2. In all the images a zoom-in on the melted section is in the inset.

While Figure 3 shows the stanogermanide formation for NiGeSn samples as a function of laser energy density, qualitatively similar features were seen in TiGeSn and PtGeSn samples. Many literature works were devoted to improve the knowledge on liquid-solid phase transformation, and the impurity behaviour in the most common group IV semiconductors [23]. Nevertheless for $Ge_{1-x}Sn_x$ this aspect has not been completely analysed yet due to the immaturity of the field [24, 25]. Since liquid-solid regrowth mechanisms govern the layer formation process, the laser energy density control is important to avoid the formation of defects, Sn segregation and misfit dislocations within the stanogermanide layer. Then LTA

thermal budget control is essential to avoid Sn cluster formation [26], and Sn surface segregation [20]. Therefore the energy density range and the sample reflectivity have to be carefully considered to successfully fabricate superior electronic devices.

From the XTEM analysis it was found that, independent of the metal used, when the LTA exceeded a threshold energy density, the stanogermanide layer tended to form two different layers, one with a vertical pillar structure and one smooth layer near the underlying $Ge_{0.91}Sn_{0.09}$. The structure obtained was in contrast with the results obtained by RTA techniques where a relatively homogeneous polycrystalline layer was observed. In literature it has been suggested that Ge undergoes amorphization and nanocrystallization under extreme thermal shock, nevertheless as the laser energy increases it can generate high stress in the melted layer, developing cracks, planar defects and grains [27]. In the samples analysed here, the misfit dislocations were generated between the Ge and GeSn layer due to the difference in the lattice parameter of these two materials. Furthermore, Demeulemeester et al. reported using real-time X-ray diffraction, that by increasing the thermal budget, Sn tends to form clusters and to segregate toward the surface [28]. Nevertheless, since the final stanogermanide layer thickness depends not only from a given energy supplied by LTA but also from several factor as metal diffusion and lattice variations; further analysis and simulations are required to outline and explain all the microscopic effects involved in the process.

Finally, to analyse the layer composition and the Sn dispersion, EDX analysis has been performed on the NiGeSn sample annealed at 500 mJ/cm^2, shown in Fig. 4. The EDX investigation along the cross section revealed that a Sn layer was localized in vertical columns or pillars in the upper part of the $Ge_{0.91}Sn_{0.09}$ layer leading to the decrease of Sn content in the middle of each cell (areas between the vertical columns of Sn). The Ni map confirms the formation of stanogermanide layer on top of the wafer.

The high angle annular dark filed (HAADF) image in Fig. 4a shows the column formation as reported in Fig. 3. EDX maps (Figs. 4b-4d) reveal the depletion of Ge in the column due to Sn accumulation, while Ni distribution is rather uniform, with a very slight increase on the top (e.g., in the Ni/Pt layer) and also in the $Ge_{0.91}Sn_{0.09}$ layer, near the Sn column. Although conclusion of the Ni omnipresence cannot be drawn definitely because the Ni EDX peak is close to the Cu peak in EDX analysis; and the latter can be seen everywhere due to the TEM sample being on a Cu grid.

White et al. reported an early work of supersaturation effects in As and Sb doped Si [29]. Subsequently Narayan et al. described a model for cell formation in Sb-Si and In-Si alloys [30]. Experimentally they observed vertical columns of Sb in sample cross-sections similar to those here. In essence as the supersaturated GeSn alloy (Sn at 9 %) is melted locally by the LTA, a liquid-solid interface is formed and, as the sample cools, then sweeps to the surface using the underlying crystal as a template. Under certain conditions the material system becomes unstable, due to the distribution coefficients of Sn and Ni in Ge, the melt depth, and the velocity of recrystallisation, where a Sn supersaturation threshold is achieved, however the excess Sn is expelled from the growing layer, in this case laterally, thus forming the vertical Sn features.

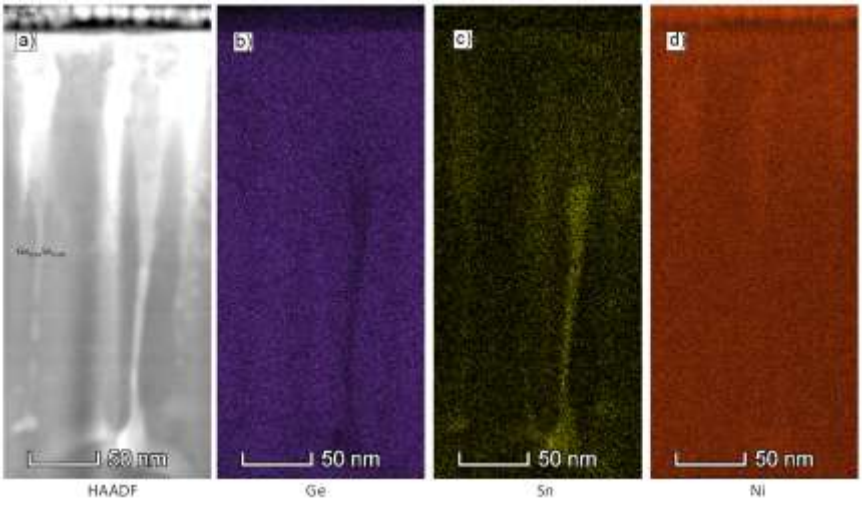


Figure 4: Representative EDX inspection for NiGeSn samples annealed at 500mJ/cm^2; the maps show respectively the HAADF, Ge, Sn and Ni maps for the column features created in the LTA process.

IV. CONCLUSIONS

In conclusion a stanogermanide contact investigation has been performed on $Ge_{0.91}Sn_{0.09}$ annealed with innovative LTA processing. As regards electrical characterization, LTA processes present a smaller resistivity fluctuation compared to RTA. XTEM and EDX analysis for LTA samples clearly highlighted the onset of Sn segregation and layer anomalies. Overall, high LTA thermal budget can cause the formation of vertical pillar structures due to lateral Sn segregation. At lower energy densities LTA can achieve low resistance stanogermanides without the extreme Sn segregation. Therefore to outperform the RTA results further, refined experiments coupled with accurate simulation are required for LTA to optimize the stanogermanide formation composition, resistance, and thickness. Finally, it is well known that silicides and germanides may have a low resistance compositional phase or a high resistance phase, therefore it would be a very insightful future study to determine information on the relationship between the stanogermanide phase versus resistance versus thermal treatment.

DECLARATION OF COMPETING INTEREST

The authors declare that they have no known competing financial interests or personal relationships that could have appeared to influence the work reported in this paper.

CRediT AUTORSHIP CONTRIBUTION STATEMENT

Emmanuele Galluccio: Investigation, Conceptualization, Methodology, Visualization, Writing - original draft. **Gioele Mirabelli:** Methodology**,** Investigation**. Alan Harvey:** Methodology, Investigation**. Michele Conroy:** Methodology, Investigation. **Enrico Napolitani:** Investigation, Writing - review & editing**. Ray Duffy:** Conceptualization, Supervision, methodology, Writing - review & editing original draft.

ACKNOWLEDGEMENTS

We acknowledge the funding support through Science Foundation Ireland Grant Number 14/IA/2513. This work was partially supported by the University of Padova (grant UNIPD-ISR 2017 ‘SENSITISE’).

References

[1] A. Reader, A. Van Ommen, P. Weijs, R. Wolters, D. Oostra, Transition metal silicides in silicon technology, Reports on Progress in Physics 56(11) (1993) 1397.

[2] S. Gaudet, C. Detavernier, A. Kellock, P. Desjardins, C. Lavoie, Thin film reaction of transition metals with germanium, Journal of Vacuum Science & Technology A: Vacuum, Surfaces, and Films 24(3) (2006) 474-485.

[3] J. Kittl, K. Opsomer, C. Torregiani, C. Demeurisse, S. Mertens, D. Brunco, M. Van Dal, A. Lauwers, Silicides and germanides for nano-CMOS applications, Materials Science and Engineering: B 154 (2008) 144-154.

[4] M. Shayesteh, K. Huet, I. Toqué-Tresonne, R. Negru, C.L. Daunt, N. Kelly, D. O'Connell, R. Yu, V. Djara, P.B. Carolan, Atomically flat low-resistive germanide contacts formed by laser thermal anneal, IEEE Transactions on Electron Devices 60(7) (2013) 2178-2185.

[5] M. Shayesteh, D. O'Connell, F. Gity, P. Murphy-Armando, R. Yu, K. Huet, I. Toqué-Tresonne, F. Cristiano, S. Boninelli, H.H. Henrichsen, Optimized laser thermal annealing on germanium for high dopant activation and low leakage current, IEEE Transactions on Electron Devices 61(12) (2014) 4047-4055.

[6] S.-H. Huang, F.-L. Lu, W.-L. Huang, C.-H. Huang, C. Liu, The 3* 10^{20} cm^{-3} Electron Concentration and Low Specific Contact Resistivity of Phosphorus-Doped Ge on Si byIn-SituChemical Vapor Deposition Doping and Laser Annealing, IEEE Electron Device Letters 36(11) (2015) 1114-1117.

[7] H. Li, H. Cheng, L. Lee, C. Lee, L. Su, Y. Suen, Electrical characteristics of Ni Ohmic contact on n-type GeSn, Applied Physics Letters 104(24) (2014) 241904.

[8] S. Wirths, R. Troitsch, G. Mussler, J. Hartmann, P. Zaumseil, T. Schroeder, S. Mantl, D. Buca, Ternary and quaternary Ni (Si) Ge (Sn) contact formation for highly strained Ge p-and n-MOSFETs, Semiconductor science and technology 30(5) (2015) 055003.

[9] C. Schulte-Braucks, E. Hofmann, S. Glass, N. von den Driesch, G. Mussler, U. Breuer, J.-M. Hartmann, P. Zaumseil, T. Schröder, Q.-T. Zhao, Schottky barrier tuning via dopant segregation in NiGeSn-GeSn contacts, Journal of Applied Physics 121(20) (2017) 205705.

[10] X. Zhang, D. Zhang, J. Zheng, Z. Liu, C. He, C. Xue, G. Zhang, C. Li, B. Cheng, Q. Wang, Formation and characterization of Ni/Al Ohmic contact on n+-type GeSn, Solid-State Electronics 114 (2015) 178-181.

[11] L. Wang, G. Han, S. Su, Q. Zhou, Y. Yang, P. Guo, W. Wang, Y. Tong, P.S.Y. Lim, B. Liu, Thermally stable multi-phase nickel-platinum stanogermanide contacts for germanium-tin channel MOSFETs, Electrochemical and Solid-State Letters 15(6) (2012) H179-H181.

[12] E. Galluccio, N. Petkov, G. Mirabelli, J. Doherty, S.-Y. Lin, F.-L. Lu, C. Liu, J.D. Holmes, R. Duffy, Formation and characterization of Ni, Pt, and Ti stanogermanide contacts on Ge0. 92Sn0. 08, Thin Solid Films 690 (2019) 137568.

[13] A. Quintero, P. Gergaud, J.-M. Hartmann, V. Reboud, E. Cassan, P.J.M.S.i.S.P. Rodriguez, Impact of alloying elements (Co, Pt) on nickel stanogermanide formation, 108 (2020) 104890.

[14] W.-J. Wan, W. Ren, X.-R. Meng, Y.-X. Ping, X. Wei, Z.-Y. Xue, W.-J. Yu, M. Zhang, Z.-F. Di, B. Zhang, Improvement of Nickel-Stanogermanide Contact Properties by Platinum Interlayer, Chinese Physics Letters 35(5) (2018) 056802.

[15] Y. Wu, W. Wang, S. Masudy-Panah, Y. Li, K. Han, L. He, Z. Zhang, D. Lei, S. Xu, Y.J.I.T.o.E.D. Kang, Sub 10^-9 Ω*cm^2 Specific Contact Resistivity (Down to 4.4x 10^-10 Ω*cm^2) for Metal Contact on Ga and Sn Surface-Segregated GeSn Film, 65(12) (2018) 5275-5281.

[16] K. Huet, I. Toqué-Tresonne, F. Mazzamuto, T. Emeraud, H. Besaucèle, Laser thermal annealing: A low thermal budget solution for advanced structures and new materials, 2014 International Workshop on Junction Technology (IWJT), IEEE, 2014, pp. 1-6.

[17] V. Mazzocchi, C. Sabatier, M. Py, K. Huet, C. Boniface, J. Barnes, L. Hutin, V. Delayer, D. Morel, M. Vinet, Boron and phosphorus dopant activation in germanium using laser annealing with and without preamorphization implant, 2009 17th International Conference on Advanced Thermal Processing of Semiconductors, IEEE, 2009, pp. 1-5.

[18] A. Firrincieli, K. Martens, R. Rooyackers, B. Vincent, E. Rosseel, E. Simoen, J. Geypen, H. Bender, C. Claeys, J. Kittl, Study of ohmic contacts to n-type Ge: Snowplow and laser activation, Applied Physics Letters 99(24) (2011) 242104.
[19] C. Carraro, R. Milazzo, F. Sgarbossa, D. Fontana, G. Maggioni, W. Raniero, D. Scarpa, L. Baldassarre, M. Ortolani, A.J.A.S.S. Andrighetto, N-type heavy doping with ultralow resistivity in Ge by Sb deposition and pulsed laser melting, 509 (2020) 145229.
[20] H. Li, Y. Cui, K. Wu, W. Tseng, H. Cheng, H. Chen, Strain relaxation and Sn segregation in GeSn epilayers under thermal treatment, Applied Physics Letters 102(25) (2013) 251907.
[21] T. Tran, Synthesis of Germanium-Tin Alloys by Ion Implantation and Pulsed Laser Melting: Towards a Group IV Direct Band Gap Semiconductor, (2017).
[22] F. Nemouchi, V. Carron, J. Lábár, L. Vandroux, Y. Morand, T. Morel, J.J.M.e. Barnes, Formation of NiGe through germanium oxide on Ge (0 0 1) substrate, 107 (2013) 178-183.
[23] F.A. Trumbore, Solid solubilities of impurity elements in germanium and silicon, Bell System Technical Journal 39(1) (1960) 205-233.
[24] S. Zaima, O. Nakatsuka, N. Taoka, M. Kurosawa, W. Takeuchi, M. Sakashita, Growth and applications of GeSn-related group-IV semiconductor materials, Science and technology of advanced materials 16(4) (2015) 043502.
[25] S. Su, B. Cheng, C. Xue, W. Wang, Q. Cao, H. Xue, W. Hu, G. Zhang, Y. Zuo, Q. Wang, GeSn pin photodetector for all telecommunication bands detection, Optics express 19(7) (2011) 6400-6405.
[26] E. Kasper, J. Werner, M. Oehme, S. Escoubas, N. Burle, J. Schulze, Growth of silicon based germanium tin alloys, Thin Solid Films 520(8) (2012) 3195-3200.
[27] S. Zhao, B. Kad, C.E. Wehrenberg, B.A. Remington, E.N. Hahn, K.L. More, M.A. Meyers, Generating gradient germanium nanostructures by shock-induced amorphization and crystallization, Proceedings of the National Academy of Sciences 114(37) (2017) 9791-9796.
[28] J. Demeulemeester, A. Schrauwen, O. Nakatsuka, S. Zaima, M. Adachi, Y. Shimura, C. Comrie, C. Fleischmann, C. Detavernier, K. Temst, Sn diffusion during Ni germanide growth on Ge1–x Sn x, Applied Physics Letters 99(21) (2011) 211905.
[29] C. White, P. Pronko, S. Wilson, B. Appleton, J. Narayan, R.J.J.o.A.P. Young, Effects of pulsed ruby-laser annealing on As and Sb implanted silicon, 50(5) (1979) 3261-3273.
[30] J. Narayan, H. Naramoto, C.J.J.o.A.P. White, Cell formation and interfacial instability in laser-annealed Si-In and Si-Sb alloys, 53(2) (1982) 912-915.